

PAPER • OPEN ACCESS

Peculiarities of the fracture upon tensile deformation of hypoeutectic silumin samples after irradiation with an intensive pulse electron beam digital image correlation method

To cite this article: Yu F Ivanov *et al* 2019 *IOP Conf. Ser.: Mater. Sci. Eng.* **665** 012005

View the [article online](#) for updates and enhancements.

Peculiarities of the fracture upon tensile deformation of hypoeutectic silumin samples after irradiation with an intensive pulse electron beam digital image correlation method

Yu F Ivanov¹, A M Ustinov^{1,2}, A A Klopotov^{2,3}, D V Zagulyaev⁴, E A Petrikova¹, Yu A. Abzaev², Yu A Vlasov², O M Loskutov²

¹Institute of High-Current Electronics SB RAS, Tomsk, 2/3 Academicheskoy Ave, 634055, Russia

²Tomsk State University of Architecture and Building, 634003, Tomsk, 2 Solyanaya Sq, 634003, Russia

³National Research Tomsk State University, Tomsk, 36, Lenin Ave, 634055, Russia

⁴Siberian State Industrial University, Novokuznetsk, 42, Kirov Street, 654080, Russia

e-mail: klopotovaa@tsuab.ru

Abstract. The deformation behavior of non-irradiated and irradiated (with an intense pulsed electron beam) samples of hypoeutectic silumin ASTMB179-92A has been investigated. The distribution of localized plasticity foci in the near-surface layers of the samples has been studied. The dependence on the state of the material (non-irradiated and irradiated samples) and the distribution of deformation fields on the surface of silumin ASTMB179-92A under tension have been revealed. A correlation between deformation stages and the evolution pattern of spatial foci of the localized deformation has been established, and the staging of deformation curves has been revealed on the non-irradiated samples. It has been shown that staging of the deformation process does not manifest itself on deformation curves of the irradiated samples. Deformation curves are characterized by a parabolic functional dependence $\sigma=f(\varepsilon)$. It has been established that irradiation with an intense pulsed electron beam leads to hardening of samples, and fracture is observed at higher values than on non-irradiated samples. A significant deformation localization in the region corresponding to the nucleation of the crack appears at stresses close to brittle failure of samples under tension.

1. Introduction

Investigation of mechanical properties of aluminum-based alloys is initiated by intensive development of many branches of modern industry [1]. Recently, methods of the material surface modification with concentrated energy fluxes, including high-energy pulsed electron beams, have been actively used in the development of alloys with an increased complex of mechanical properties [2]. As a rule, modification of the surface layer of a material with concentrated energy fluxes is accompanied by formation of a gradient structure, the properties of which depend on the distance to the treatment surface. This circumstance significantly complicates the analysis of the deformation process of such materials. One of the directions for the analysis of the localization of plastic deformation of the material at meso- and macro-scale levels is the speckle interferometry [3], implemented in works [4, 5] with the use of a three-dimensional digital optical system Vic-3D.

The purpose of the article is to identify and analyze distribution patterns of local deformation foci under tensile conditions of flat samples from hypoeutectic silumin ASTMB179-92A in the initial, and the irradiated with an intense pulsed electron beam, states.

2. Materials and methods of the experiment



Samples of ASTMB179-92A silumin were the research material. Proportional flat samples with a tail for cantilever fastening were used in tensile tests. Test samples were divided into two batches. The first batch consisted of silumin samples in a cast state. The samples of the second batch were additionally irradiated with an intense pulsed electron beam using the SOLO installation [6] with the following parameters: the pulse duration of the electron beam is 150 μs , the number of pulses is 3, the pulse repetition rate is 0.3 s^{-1} , the electron beam energy density is 25 J/cm^2 .

The tensile test was carried out using an INSTRON 3386 testing machine. The deformation rate was constant and was equal to 2 mm/min. The deformation distribution in the near-surface layers of the sample under tension was obtained using the VIC-3D optical measuring system [7, 8]. The image recording scheme on the surface of samples for obtaining digital stereoscopic images under tension is shown in figure 1. Before tests, speckle structures were created on the surface of samples with contrasting fine white and black matte aerosol paints. Changes in displacement fields during the deformation process in real time were obtained based on processing of digital stereoscopic images using the VIC-3D optical measuring system. These displacement fields represent displacement projections of local regions of the sample surface along the OX axis (transverse deformation) and along the OY axis (longitudinal deformation). During further processing, using the software of the VIC-3D system, the displacements were converted to relative deformations (ϵ_{xx} is along the X axis, ϵ_{yy} is along the Y axis, ϵ_{xy} is the shear deformation). The deformation pattern of the sample surface is obtained by combining changes in microregions. Structural studies of the surface of the ASTMB179-92A alloy were carried out using scanning electron microscopy (LEO EVO 50 (Zeiss, Germany)).

3. Research results and discussion

The structure of ASTMB179-92A silumin in the cast state is characterized by the presence of micropores, inclusions of intermetallides and silicon of micron sizes (figure 2). The presence of micropores and inclusions (especially plate-shaped) contributes to embrittlement of the alloy.

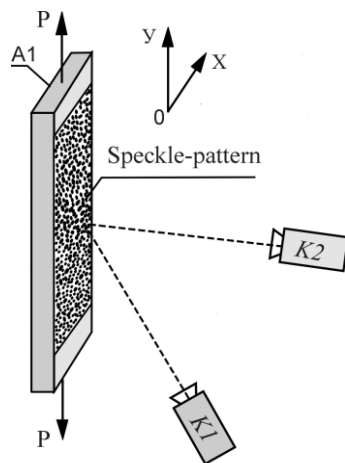


Figure 1. The scheme of image registration of the a speckle pattern on the lateral surface of the sample under tension; K1 and K2 are digital cameras; P is the applied load.

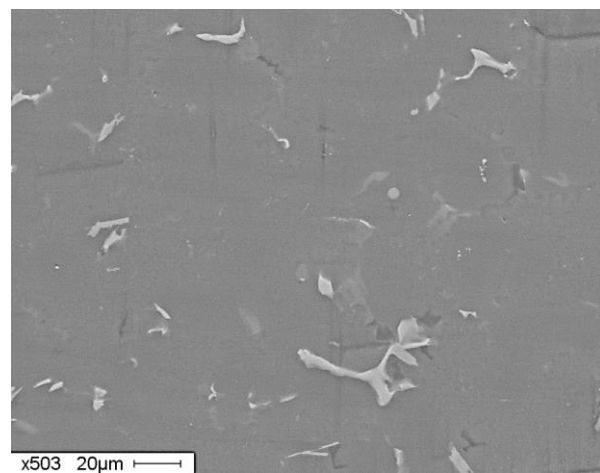


Figure 2. The surface structure of the hypoeutectic silumin ASTMB179-92A sample, identified using methods of scanning electron microscopy. The initial state.

First tensile stage (figure 3, *a*, stage I) is characterized by elastic deformation. At this stage, in distribution patterns of horizontal and vertical relative deformations, plastic deformation foci are localized in small regions of the sample surface (figure 4). Points 1 and 2 on the deformation curve $\sigma=f(\epsilon)$ at stage I (figure 3) correspond to the distribution pattern of horizontal and vertical relative deformations on the silumin plate surface (figure 4). These regions are randomly located along the surface of the sample with the presence of both positive and negative values. A combined local deformation foci ϵ_{yy} with compression and tension regions (pattern 1, figure 4) has formed in the central

part of the sample, which then, with increasing applied external stress, has transformed into a local deformation foci of only tension (pattern 4, figure 4).

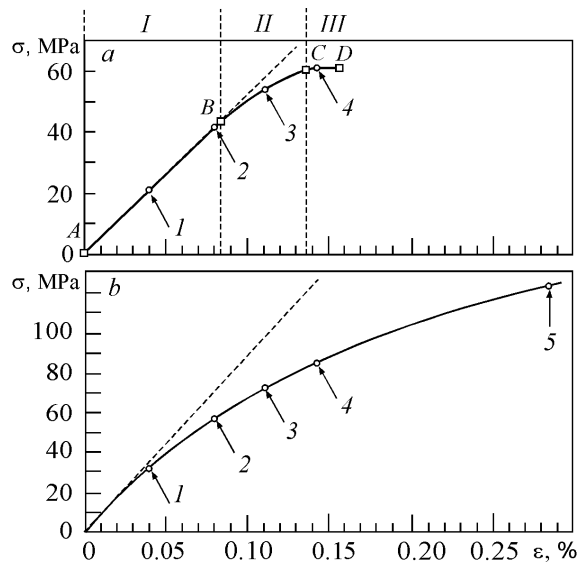


Figure 3. Deformation diagrams of non-irradiated (a) and irradiated (b) silumin with an intense pulsed electron beam. The numbers correspond to position of the deformation structure patterns on the curve (figure 4 and figure 5). AB is the stage of elastic deformation (stage I); BC is the transitional stage (stage II); CD is the stage of deformation softening (stage III) and fracture.

stage reaches values of $\sim 0.09\%$ under tension of non-irradiated samples of hypoeutectic silumin ASTMB179-92A. In the literature, the margin for residual deformation for steels and aluminum alloys is usually 0.2% (plastic deformation is 0.002) [9]. Thus, the obtained results characterize the investigated silumin as very fragile.

Further analysis of the obtained results has been carried out on the basis of constructing deformation diagrams for maximum values of vertical and horizontal deformations inside plastic deformation foci on the surface of the samples (figure 5). The deformation diagram, with respect to maximum values of vertical deformations inside plastic deformation foci on the surface of the samples under tension, has a functional dependence $\sigma=f(\varepsilon_{YY})$, close to parabolic (with the exception of the section AB, figure 5, a). Plastic deformation of the material in these foci is more than 3 times greater than the average deformation of the sample at the last stage III.

The deformation diagram, with respect to maximum values of horizontal deformations inside plastic deformation foci on the surface of the samples under tension, is shown in figure 5, b. It is characteristic that the functional dependence $\sigma=f(\varepsilon_{XX})$ can be represented as two linear segments AC and CD.

The stress at point C in the diagram (figure 5, b) coincides with the stress in the deformation diagram of the alloy under study, at which the transition from stage II to stage III begins (point C, figure 3) and correlates with the stress at point C in the deformation diagram, relative to maximum values of vertical deformations (figure 5, a).

Thus, a difference in functional dependences $\sigma=f(\varepsilon_{YY})$ and $\sigma=f(\varepsilon_{XX})$ of deformations in plastic deformation foci has been revealed during tensile deformation of cast silumin samples. The dependence of the deformation behavior of the material on the deformation direction has been revealed.

Distribution of deformations ε_{YY} in the vertical direction along the OY axis changes at stage II (figure 3, a). Individual plastic deformation foci merge in the lower and upper parts of the samples, (pattern 3, figure 4). Moreover, at stage II, plastic deformation foci (with $\varepsilon_{YY}<0$) almost completely disappear, and plastic deformation foci (with $\varepsilon_{YY}>0$) remain (figure 4).

The analysis of ε_{XX} deformation distribution patterns in the horizontal direction shows that the local deformation foci along the OX axis have an elongated shape, mainly in the direction along the vertical axis of the sample (the OY axis, figure 1). While foci of relative local deformation ε_{YY} have an elongated shape, mainly in the direction perpendicular to the vertical axis of the sample (axis OX, figure 1).

Transition from stage II to stage III ends with the fracture of the sample (figure 3, a). At stage III, in the central part of the sample, the deformation ε_{YY} in the local focus is more than twice the average deformation over the entire sample. Further destruction of the sample occurs in this area.

It has been shown that elastic deformation

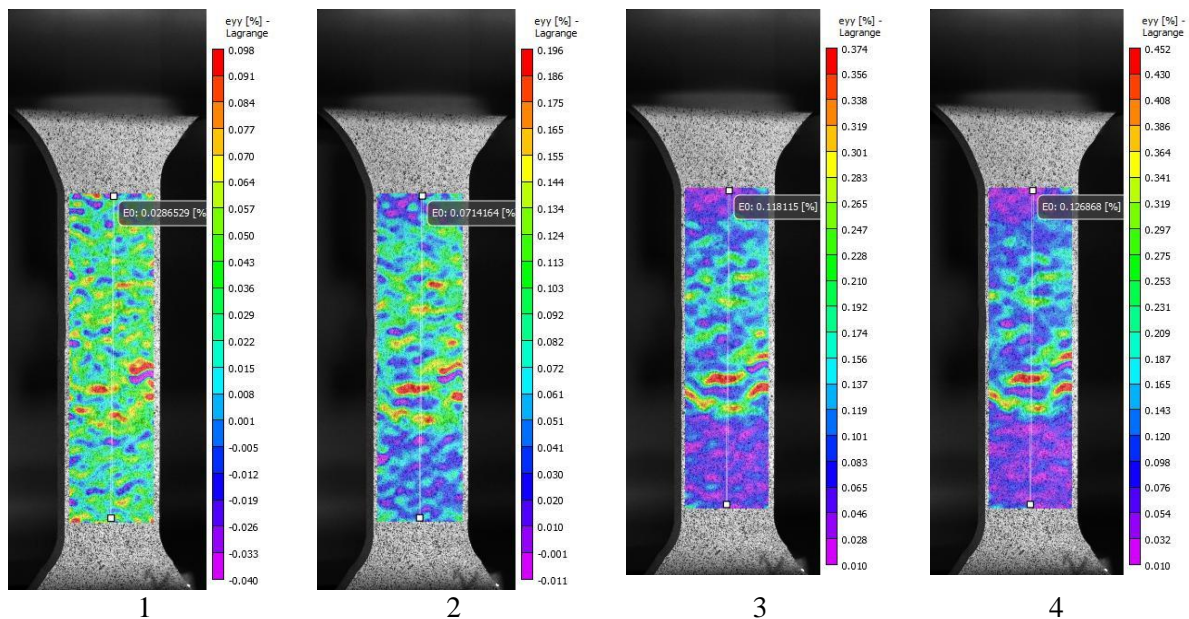


Figure 4. Distribution patterns of vertical relative deformations on the surface of a flat plate of cast silumin ASTMB179-92A. Figures 1, 2, 3, 4 in the diagram in figure 3 *a* show the corresponding strain-stress states of the sample during the test.

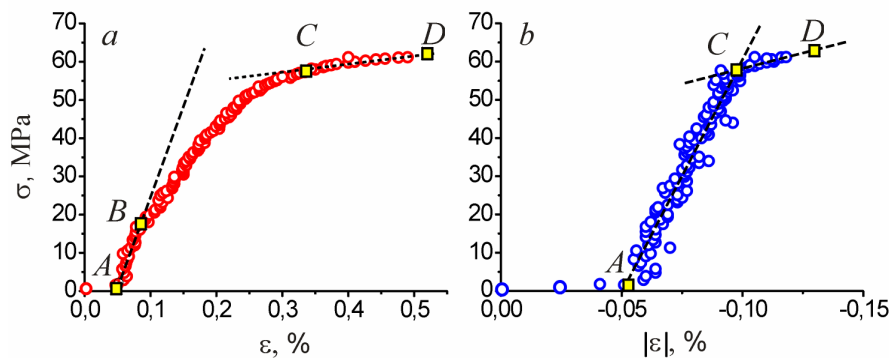


Figure 5. Deformation diagrams, with respect to maximum values of vertical $\sigma=f(\varepsilon_{YY})$ (*a*) and horizontal $\sigma=f(\varepsilon_{XX})$ (*b*) deformations inside plastic deformation foci on the surface of non-irradiated silumin samples under tension. AB and AC are linear sections on the dependences $\sigma - \varepsilon$ and $\sigma - |\varepsilon|$, respectively.

The above mentioned patterns (figure 4) of relative deformation distributions on the surface of a flat plate in the middle part of the sample clearly exhibit significant plastic deformation foci beginning from ~ 20 MPa. This phenomenon reflects the development of the plastic deformation localization in this particular part of the sample. With further tension, the appearance of plastic deformation foci in other parts of the sample suggests that stress concentrators exist in these places in the sample. However, an increase in the applied voltage leads to development of the local deformation region in the central part of the sample (figure 4). Ultimately, this leads to formation of cracks and brittle fracture of the sample as a whole.

The results of the tensile test of the irradiated sample of ASTMB179-92A silumin are shown in figure 3 *b*. The resulting diagram is characterized by a parabolic functional dependence $\sigma=f(\varepsilon)$ [10]. It is impossible to single out deformation stages, as it had been done on the deformation curve of the non-irradiated sample (figure 3, *a*). Irradiation with an intense pulsed electron beam leads to sample

hardening, and fracture is observed at higher values than on non-irradiated samples. At stresses close to brittle failure of the samples under tension, in the formed localization foci of the plastic deformation, the value of the plastic deformation in horizontal direction (along the OX axis, figure 6, *d*) is close to total deformation of the entire sample. Whereas, in plastic deformation localization foci on the sample surface in the vertical direction (along the OY axis, figure 6, *c*), the magnitude of plastic deformation values is significantly less than the total deformation.

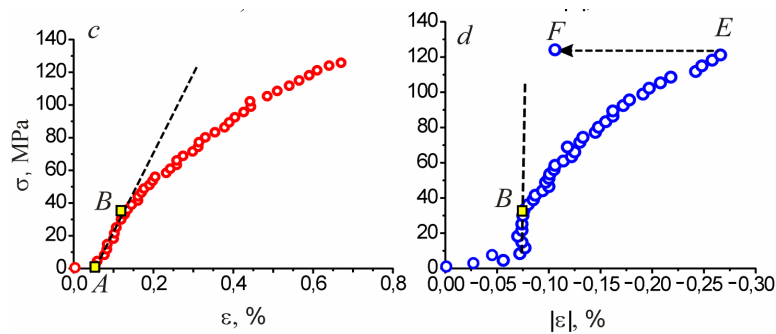


Figure 6. Deformation diagrams for maximum values of vertical $\sigma=f(\epsilon_{YY})$ (*c*) and horizontal $\sigma=f(\epsilon_{XX})$ (*d*) deformations inside plastic deformation foci on the surface of irradiated silumin samples under tension. AB and AC are linear sections on dependences σ from ϵ and σ from $|\epsilon|$, respectively. EF is the line reflecting the stage of a sample fracture on the irradiated sample.

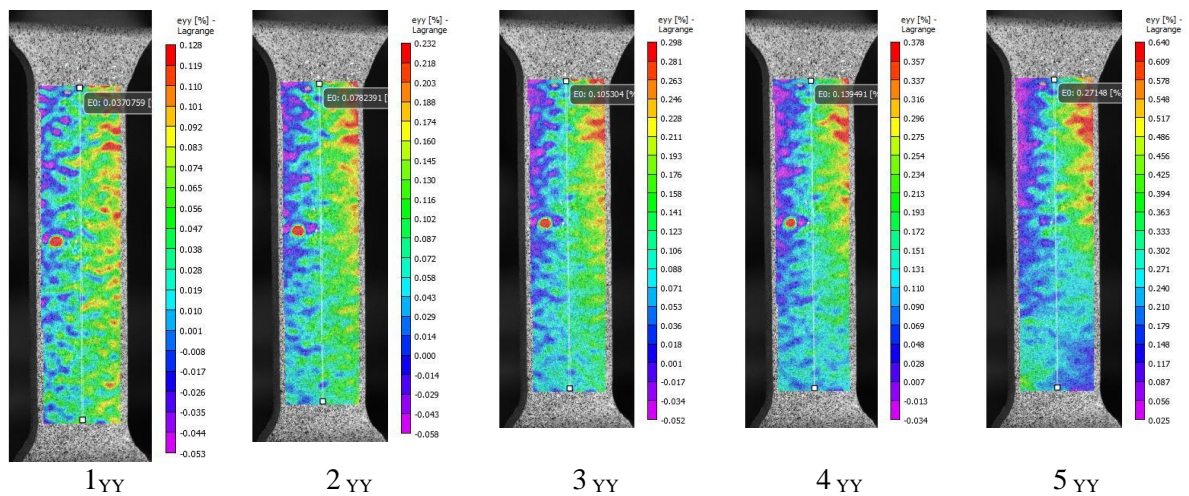


Figure 7. Distribution patterns of vertical relative deformations on the surface of a flat plate of the irradiated silumin ASTMB179-92A. Numbers 1, 2, 3, 4, 5 in the diagram show in figure 3, *b* the corresponding strain-stress states of the sample under test.

The staging of the plastic flow curve is associated with the nature of the plastic deformation localization [11]. It is impossible to distinguish individual stages for the non-irradiated alloy on the deformation curve, which is reflected in a similar form of deformation distribution patterns on the sample surface (figure 3, *b* and figure 7).

It is obvious that such an evolution of deformation patterns of the deformation distribution on the surface of the irradiated sample in the process of tensile deformation reflects the presence of a hardened surface layer on the sample [12]. When studying deformation maps, it can be seen that the elastic deformation foci, which then transforms into plastic deformation foci, are localized at the initial moment on the lateral faces of the sample. Further, fusion of these plastic deformation foci is observed with an

increase in the applied stress. As a result, the deformation field in one of the largest deformation foci becomes critical, which leads to formation of a crack and fracture of the sample (figure 7, pattern 5).

For the irradiated alloys, deformation diagrams for maximum values of vertical $\sigma=f(\varepsilon_{YY})$ and horizontal $\sigma=f(\varepsilon_{XX})$ deformations inside plastic deformation foci on the surface of the samples (figure 6 *c, d*) have been plotted. It can be seen that the initial stage includes a linear dependency $\sigma=f(\varepsilon_{YY})$ which ends at a voltage of ~35 MPa. However, in the non-irradiated sample, the linear dependence region ends at lower values of ~ 18 MPa. The end of the linear region of the dependence on the curve $\sigma=f(\varepsilon_{YY})$ correlates with the end of the vertical region on the dependence $\sigma=f(\varepsilon_{XX})$ (point B, figure 6 *c, d*). The functional dependence close to parabolic begins with a voltage of ~ 35 MPa on the curve $\sigma=f(\varepsilon_{YY})$ (point B).

The maximum deformation in the vertical direction in the irradiated alloy in the plastic deformation foci before fracture is 2 times higher than the average deformation in the sample. The maximum deformation in the horizontal direction in plastic deformation foci before fracture is close to the average deformation in the sample (figure 3 and figure 6 *c, d*). The fracture process includes sample unloading, and the maximum deformation in the deformation foci on the sample surface in the horizontal direction ε_{XX} considerably decreases (figure 6, *d*, point F).

Thus, for the irradiated alloy, in contrast to the non-irradiated, similar functional dependences $\sigma=f(\varepsilon_{YY})$ and $\sigma=f(\varepsilon_{XX})$ of deformations in plastic deformation foci on the sample surface have been established depending on the direction of deformation.

4. Conclusion

Three deformation stages have been revealed on tensile diagrams $\sigma=f(\varepsilon)$ of the non-irradiated hypoeutectic silumin ASTM B179-92A. The elastic deformation stage (stage I) ends at deformation of ~0.09%, transition from stage II to III at deformation of ~0.14%, sample fracture occurs at $\varepsilon_{\text{time}} \sim 0.16\%$. Transition from stage I to II on the deformation curve is manifested in the fact that deformation distribution patterns, in the vertical direction in stage II, almost completely lack plastic deformation foci, in which $\varepsilon_{YY} < 0$, and the plastic deformation foci, in which $\varepsilon_{YY} > 0$, remain. Whereas, at stage I, plastic deformation of compression and tension does exist. A correlation in the evolution of distribution patterns of horizontal and vertical relative deformations on the surface with stages in the deformation dependence $\sigma=f(\varepsilon)$ under tension of non-irradiated samples has been established. The local deformation inside plastic deformation foci in the vertical direction at the pre-fracture stage is 3 times higher than the average deformation over the entire sample. Irradiation of the surface of hypoeutectic silumin ASTM B179-92A samples results in a twofold increase in the magnitude of the fracture stress of the sample, as compared to the unirradiated sample. Investigations of deformation diagrams $\sigma=f(\varepsilon)$ of irradiated hypoeutectic ASTM B179-92A silumin under tension has not allowed to single out stages. This type of deformation curve correlates with distribution of strain fields on the sample surface: distribution patterns of relative deformations on the surface of the irradiated sample are similar to patterns when the sample is deformed from 0.04% to 0.28%.

Acknowledgement

The research was financially supported by the RSF (project No 19-79-10059).

5. References

1. Fridlander I N 2006 *Memories on the development of aerospace and nuclear technology from aluminum alloys* (Moscow: Nauka).
2. Ivanov Yu F 2017 *Russian Physics Journal* **60** No. 1 175-81.
3. Ustinov A M et al 2018 *Materials Science Forum* **938** 62-9.
4. Kopanitsa D G et al 2018 *Russian Physics Journal* **60** No. 9 177-85.
5. Jones R, Wykes C 1983 *Holographic and Speckle Interferometry* (Cambridge: University Press).
6. Koval N N and Ivanov Yu F 2008 *Russian Physics Journal* **51** No. 5 60-70.

7. Manalo A et al 2016 *Construction and Building Materials* **105** 365–76.
8. Vildeman V E et al 2017 *Mechanics of Solids* **52** No 5 488-94.
9. Panin V E 1998 *Theor. & Appl. Fract. Mech.* **30**. No1 1-12.
10. Derugin E E 2003 *Fatigue Fract. Engng Mater. Struct.* **26** 295-304.
11. Honeycombe R W K 1984 *The plastic deformation of metals*. Edward Arnold. 1984, 483 p.
12. Polukhin P I, Gorelik S S and Vorontsov V K 1982 *Physical basis of plastic deformation* (Moscow: Metallurgy).